

## Article

# A Support Vector Machine Hydrometeor Classification Algorithm for Dual-Polarization Radar

Nicoletta Roberto <sup>1,\*</sup>, Luca Baldini <sup>1</sup>, Elisa Adirosi <sup>1,2</sup>, Luca Facheris <sup>3</sup>, Fabrizio Cuccoli <sup>2</sup>, Alberto Lupidi <sup>2,4</sup>  and Andrea Garzelli <sup>5</sup> 

<sup>1</sup> National Research Council of Italy (CNR), Institute of Atmospheric Sciences and Climate (ISAC), Rome 00133, Italy; l.baldini@isac.cnr.it (L.B.); e.adirosi@isac.cnr.it (E.A.)

<sup>2</sup> National Laboratory of Radar Surveillance System (RaSS), Interuniversity Consortium for Telecommunication (CNIT), Pisa 56124, Italy; fabrizio.cuccoli@unifi.it (F.C.); alberto.lupidi@iet.unipi.it (A.L.)

<sup>3</sup> Department of Information Engineering, University of Florence, Florence 50139, Italy; luca.facheris@unifi.it

<sup>4</sup> Department of Information Engineering, University of Pisa, Pisa 56122, Italy

<sup>5</sup> Department of Information Engineering, University of Siena, Siena 53100, Italy; andrea.garzelli@unisi.it

\* Correspondence: n.roberto@isac.cnr.it; Tel.: +39-06-4993-24326

Received: 21 June 2017; Accepted: 20 July 2017; Published: 25 July 2017

**Abstract:** An algorithm based on a support vector machine (SVM) is proposed for hydrometeor classification. The training phase is driven by the output of a fuzzy logic hydrometeor classification algorithm, i.e., the most popular approach for hydrometer classification algorithms used for ground-based weather radar. The performance of SVM is evaluated by resorting to a weather scenario, generated by a weather model; the corresponding radar measurements are obtained by simulation and by comparing results of SVM classification with those obtained by a fuzzy logic classifier. Results based on the weather model and simulations show a higher accuracy of the SVM classification. Objective comparison of the two classifiers applied to real radar data shows that SVM classification maps are spatially more homogenous (textural indices, energy, and homogeneity increases by 21% and 12% respectively) and do not present non-classified data. The improvements found by SVM classifier, even though it is applied pixel-by-pixel, can be attributed to its ability to learn from the entire hyperspace of radar measurements and to the accurate training. The reliability of results and higher computing performance make SVM attractive for some challenging tasks such as its implementation in Decision Support Systems for helping pilots to make optimal decisions about changes in the flight route caused by unexpected adverse weather.

**Keywords:** dual polarization; weather radar; support vector machine; hydrometeor classification algorithm; fuzzy logic

## 1. Introduction

During the last few decades, most worldwide weather radar infrastructure has been upgraded to dual-polarization. New meteorological products and applications based on dual-polarization radar measurements have been proposed and made available to end users, like weather services, to improve precipitation estimation and better understand the nature of precipitating clouds for predicting their evolution in the short term. Among these products, the identification of hydrometeor type has become one of the most popular, having attracted the interest of researchers and weather radar users. Different Hydrometeor Classification Algorithms (HCA) have been proposed so far. Most of the HCAs implemented at operational radars are based on empirical approaches, allowing us to deal with approximate knowledge of the actual relationships between radar measurements and precipitation microphysics such as the fuzzy logic (FL) methods (see [1–5] among others), but there are also algorithms based on a Bayesian approach [6]. Typically, HCAs classify hydrometeors by analyzing the set of dual-polarization measurements pertinent

to a single radar measurement volume. Most of the recent literature on fuzzy logic HCA aimed at improving the membership functions (e.g., [7]) also focusing on specific classes [8,9]. Steps forward to improve the robustness of the fuzzy logic approach are the semi-supervised approach in [10], which improved the spatial coherency of classification maps by exploiting measurements in the neighboring bins, and the unsupervised clustering approach [11] to define the number of classes and the membership functions. More recently, a semi-supervised approach, that exploits fuzzy logic approach for defining the constraints of an unsupervised approach was presented [12].

Supervised learning models based on a Support Vector Machine (SVM) are widely used for classifying different remote sensing imageries (see [13] for a review), including meteorological satellite observations (e.g., [14]). Therefore, the SVM approach is worth investigating for hydrometeor classification using dual-polarization radar measurements. Actually, a few HCA implementations based on supervised learning methods can be found in the literature. Neural networks have been used in [1] to automatically adjust membership functions based on observed data and fuzzy logic classification results, while in [15] an SVM model has been used as part of a hydrometeor classification scheme to define hydrometeor classes based on 2D Video disdrometer measurements.

The development of the SVM hydrometeor classification algorithm illustrated in this paper was stimulated by research and development projects funded in the framework of the Clean Sky Joint Technology Initiative (JTI) of the European Commission ([www.cleansky.eu](http://www.cleansky.eu)). Such projects aimed at improving the state of the art of the weather radars used on-board civil aircrafts to detect adverse weather during the flight. Current systems are pulsed single polarization X-bands radars that estimate the effective radar reflectivity factor. This is then displayed in a few colors according to the specific standards, where, typically, areas in red on the pilot's display need to be avoided. Some radar systems have Doppler capabilities and allow, within a certain distance, the detection of turbulence associated with the motion of cloud particles. Dual polarization offers several appealing advantages for civil aircraft applications. The main advantage is the ability to compensate for the X-band attenuation due to precipitation, thus avoiding to underestimate the risk associated with convective cells. Moreover, the possibility of implementing automated hydrometeor classification procedures to detect the presence of dangerous weather conditions such as that characterized by the presence of hydrometeors like hail or graupel, typically associated with convection, and improving pilot awareness of weather along the route [16]. A scheme of a possible radar data processing on a specific avionic device (the Electronic Flight Bag) that includes a hydrometeor classification module is described in Appendix A. The procedure for classifying hydrometeors based on avionic weather radar (AWR) measurements needs to satisfy some strict requirements in terms of computing time. It was noticed that SVM algorithms perform better from the computational point of view than fuzzy logic. A benchmark test comparing fuzzy logic and SVM classification algorithms was performed; in particular, computational time (namely the number of labels per second) has been tested on a machine running a Linux operating system (details in Appendix A). However, the SVM HCA developed and shown in this paper is generic and can be effectively used for ground-based weather radar. In fact, evaluation shown in Section 4 is applied to dual-polarization ground-based X- and C-band weather radar.

The major implementation problem of the SVM classifier is the learning phase. In fact, performance in classification is strictly dependent on relationships between input variables and class labels, established during the learning phase. For the case of hydrometeor classification, this process has been implemented with the support of results obtained by a fuzzy logic classifier. In case of quasi-real-time classification product, the learning phase is performed offline, reducing the calculation time.

A further challenging task in HCA development is the evaluation of the performance. In fact, it is difficult and expensive to collect independent and coincident measurements of hydrometeors within a radar resolution volume [17,18]. Even when these measurements are available, the comparison is not easy at all due to the different nature of the measurements involved, such as the radar measurements relative to a wide resolution volume and reference measurements collected by a probe on a research aircraft that samples a much smaller volume. Consequently, most of the validation examples reported

in the literature are qualitative (e.g., in [7,11]). In this paper, the output of the Weather Research and Forecast (WRF) model with an explicit microphysics scheme is used, jointly with simulation of weather radar measurements, with the objective to validate SVM HCA [18–20]. This approach is applied to a real weather scenario obtained from an intense convective event that occurred on 15 October 2012 in the Southern Mediterranean. The WRF microphysics output is considered the truth reference for validating the SVM HCA output, where synthetic weather radar measurements are used as input. Such an analysis also allows us to investigate important aspects related to the SVM implementation of HCA, such as the size of the training set. Finally, the SVM HCA is tested on real data collected by a C-band and an X-band dual-polarization ground-based radar. The C-band datasets consist of 16 case studies of intense convective events observed by the C-band Doppler dual polarization radar Polar 55C located in Rome, Italy in 2012 and 2015. The second dataset includes two intense precipitation events that occurred in 2013 in Sicily, observed by the X-band dual-polarization radar of the airport in Catania, Italy.

The paper is structured as follows: Section 2 recalls the concepts of support vector machine classification and its implementation based on a working fuzzy logic classifier; Section 3 illustrates the validation of the approach based on a precipitation microphysics scenario produced by a weather model that is used as a true reference for investigating the performance of the SVM classifier. Evaluation of the performance of the SVM classifier, with respect to the corresponding fuzzy logic classifier by means of weather radar measurements collected at C and X-band is then shown in Section 4. Finally, the main results found are summarized in Section 5.

## 2. The SVM Hydrometeor Classification Algorithm

### 2.1. Support Vector Machine Description

Machine learning approaches and supervised models like SVM are used to establish an input–output relationship directly from the data, with no a priori assumptions. Briefly, an SVM classification algorithm consists of two phases: the training phase, in which the relationship between input variables (i.e., radar measurements) and class labels output (i.e., hydrometeor classes) is established, and the prediction phase, in which the most likely class is assigned to input sample measurements. Although updates are possible, the supervised algorithm is trained once and the training is performed outside of the classification prediction scheme: once training is complete, classification prediction can work with a reduced computational time. These characteristics make machine learning models very competitive in terms of applicability to a wide range of problems that require high classification speed.

The SVM classifier usually proceeds for the two-class problem in three stages. The first one is the *basic margin classifier*, where separation between two classes is tested with a linear decision boundary (a hyperplane). For problems that are not separable by a linear decision, a second step is performed in which the classifier is modified to tolerate misclassification (*soft margin*) by introducing a penalty. At the last stage, the classifier can be nonlinearly generalized by using a *kernel method*. In our case, the samples are the set of radar measurements related to each radar resolution volume, while the classes are the types of hydrometeor dominant in a radar resolution volume and can be classified.

An SVM model classifies samples by finding the best hyperplane that separates all data points of one class from those of the other class with the largest margin between the two classes. Therefore the margin can be defined as the maximal width of the slab parallel to the hyperplane that has no internal data points. The support vectors ( $w$ ) are the data points that are closest to the separating hyperplane. Finding the support vectors corresponds to solve a primal-dual problem [21]. When samples cannot be completely separated by a hyperplane, SVM can use a soft margin (the second step defined above) determining a hyperplane separating a significant number of samples. The typical approach used in SVM to solve the non-linear problem is to make use of the kernel formulation. In this work, the kernel is a radial basis function (RBF).

All the calculations for hyperplane classification do not use more than inner products. Therefore, nonlinear kernels can use identical calculations and solution algorithms, and obtain classifiers that are nonlinear. The resulting classifiers are hypersurfaces in some space  $S$ , but the space  $S$  does not have to be identified or examined [22,23].

In its basic form, the support vector machine [21] is a linear classifier, which finds the best linear separation between samples belonging to two classes. This binary scheme can be extended for multiclass classification by combining several binary classifiers, while one-step multiclass solutions are generally more computationally expensive. An accurate strategy used for this purpose is the one-against-all (OAA) [24] that is used in this work to obtain six hydrometeor classes. The OAA method consists of applying binary SVM to separate members of one class from members of other classes. The algorithm is based on a parallel architecture composed by  $N$  SVMs, one for each class.

To build the hydrometeor classification based on SVM, the LIBSVM library [25] has been used. It is composed of a set of libraries written in C and Python languages and run by a MATLAB script for training and validating SVM (software run on a 64-bit Linux Red Hat 4.4.7-4 machine). Following the processing chain of civil aircraft radar shown in Appendix A, the SVM training output is preloaded and the prediction phase need low computational performance. The Electronic Flight Bag (EFB) product, running a Certified Linux Operating System, DO178 Level C, is enough to run the SVM predict phase (see details of EFB characteristics in Table A1).

## 2.2. Support Vector Machine Implementation of HCA

The SVM training phase provides the grounds of the algorithm: the support vectors are defined through some unknown linear relations between observations for which labels are known. Thus, going through this phase is critical to the performance of the predict phase and, in the case of hydrometeor classification, it could involve processing of large sets of data. Since fuzzy logic is a rather popular approach for HCA, a FL-HCA is used to support the training phase. Fuzzy logic HCAs differ from each other because of input and output sets (radar measurements and hydrometeor classes, in our case), and membership functions that, calculated for each class for each radar-sampled volume, define the degree of truth of the class of hydrometeor. They can be determined both by investigating physical scattering and propagation behavior of the different hydrometeors and by analyzing empirical measurements. The FL-HCA used in this paper is that used at the Institute of Atmospheric Sciences and Climate of the Italian National Research Council (ISAC-CNR) [26]. It is mostly based on [17] and is tailored to identify meteorological targets, with a particular emphasis on the hydrometeors involved in convective events. Recent updates are described in [9,27], for X-band and C-band, respectively, that show the membership functions used. Such functions are not so different from those reported in the literature and therefore the results obtained should not be significantly influenced by the choice of FL classifier. Input measurements are reflectivity factor ( $Z_h$ ), differential reflectivity ( $Z_{dr}$ ), specific differential phase shift ( $K_{dp}$ ), copolar correlation coefficient ( $\rho_{hv}$ ) [28], and the height of the  $0^\circ$  isothermal. For the C-band validation, the standard deviation of differential phase shift  $\sigma(\Phi_{dp})$  substitutes the copolar correlation coefficient. The output set comprises the six classes of hydrometeors described below:

- *Rain*: this class includes, light rain, moderate rain and heavy rain (characteristics of convective events). For this reason,  $Z_h$  spans from 10 to 60 dBZ and  $Z_{dr}$  assumes positive values due to the oblate shape of rain. The liquid hydrometeors are typically detectable below the melting layer (ML).
- *Dry Snow*: this class includes all the non-wet ice particles, such as aggregates, plates, and columns, which determine the relatively low values of  $Z_h$ . Such particles are typically detectable above the ML.
- *Wet Snow*: this class typically refers to ice particles in the melting phase, which typically present in the ML. These hydrometeors are usually ice particles or aggregated ice particles covered by a film of water that result in high values of  $Z_h$ .

- *Graupel*: these hydrometeors are detectable both above and within the melting layer: usually these particles melt below the ML, but they may reach the ground during convective events with intense downdraft. They are smaller than hail and thus are associated with  $Z_h$  values lower than those found in hail. They produce  $Z_{dr}$  levels around 0, but conical graupel can produce negative  $Z_{dr}$  values.
- *Hail*: the presence of hailstones characterizes convective events. They are typically found in the core of the deep convective cells and are detectable from the ground up to several kilometers above the ML. The updraft of the convective cell drives the growth of these particles, whose dimensions can reach the order of centimeters. Hailstones have high variability in their size and shape distribution. A typical signature of these particles is high values of  $Z_h$  and  $Z_{dr}$  and  $K_{dp}$  values around 0 (due to tumbling).
- *Hail Mix*: these hydrometeors occur from ground to few kilometers above the ML. The hydrometeors in this class are representative of a mix, present within the radar resolution volume, of raindrops lifted by updraft, supercooled raindrops, hail, small hail, and graupel. The typical signature is high values of  $Z_h$  and low values of  $\rho_{hv}$  (these values decrease for the increase of hail amount of different size and increases with increasing mixing) while  $Z_{dr}$  spans from negative to positive values.

Since the training phase of the SVM is the core of the HCA set-up, the training set should be as representative as possible of the physical phenomena to be classified. For this purpose, a large number of cases, including different types of meteorological events, have to be included in the training set. The given set of available weather radar observations is divided into two subsets: the first is selected to perform the training phase, namely training observations ( $l$ ), while the other one consists of the test observations ( $m$ ).

A few processing steps are necessary to run both the SVM and FL HCAs:

1. *Unreliable data removal*. pixel affected by ground clutter, anomalous propagation, and non-meteorological targets were identified and removed by applying a set of thresholds on  $Z_h$  and on the standard deviations of  $\phi_{dp}$  and  $Z_{dr}$  [28].
2. *Estimation of specific differential phase*. Different methods are used to estimate  $K_{dp}$  from differential phase shift measurements. For C-band datasets,  $K_{dp}$  is estimated using the finite difference method [28], while for X-band datasets an iterative moving-window range scheme was adopted [29].
3. *Attenuation correction for  $Z_h$  and  $Z_{dr}$* . Measurements propagated along paths below the  $0^\circ\text{C}$  level are corrected using a linear relation of  $K_{dp}$  with specific attenuation and specific differential attenuation ( $A_h$ ,  $A_{dp}$ , respectively) i.e.,  $A_{h,dp} = \gamma_{h,dp} K_{dp}$ . The parameterizations adopted to obtain  $\gamma_{h,dp}$  coefficients at X-band and C-band are performed by T-matrix scattering simulations using three years of disdrometer observations collected in Rome by a disdrometer [30].
4. *Correction of polarimetric variables for elevation angle*. The values of the polarimetric variables of the same ensemble of scatterers change with the elevation angle. The most affected are  $Z_{dr}$  and  $K_{dp}$ , while  $Z_h$  typically does not change more than 1 dBZ, which is the intrinsic uncertainty due to noise. In general,  $Z_{dr}$  and  $K_{dp}$  exhibit their maxima at  $0^\circ$  elevation and their values gradually decrease to 0 when reaching vertical incidence. In this work,  $Z_{dr}$  and  $K_{dp}$  are corrected for elevation angles by recalculating their values as observed at  $0^\circ$  of elevation [31].
5. *Estimation of  $0^\circ\text{C}$  level*. The  $0^\circ\text{C}$  level is estimated using vertical profiling soundings from the closest sounding station. If the processing is referred to the AWR, this level can be estimated directly from measurements collected by devices on-board an airplane.
6. *Input SVM data organization*. The dual-polarization measurements  $Z_h$ ,  $Z_{dr}$ ,  $K_{dp}$ , and  $\rho_{hv}$  (or  $\sigma(\Phi_{dp})$  at C-band) and the height of  $0^\circ$  level are stored in an organized structure. The organization for the data access is made by n-tuples (a row of the whole structure contains a single n-tuple of polarimetric features).

The SVM algorithm is trained on classification maps generated by a FL classification approach. For each class the SVM descriptors (organized in the so-called support vector, SV) are extracted. In the



case of operational classification, on the ground or during flight, the training is performed off the processing chain. Before performing the training procedure, input data are prepared. A training set is made up of a certain number ( $l$ ) of  $n$ -tuples, depending on the accuracy needed by the user and on the related computational load (the higher the number of  $n$ -tuples, the more time required by the training phase). Furthermore, the data are scaled into a specific range. This step is necessary because, in general, the input features contained in each  $n$ -tuple may have values of different scales and therefore are not commensurable. The scaling of the data is performed on the test set as well as on the training set.

Furthermore, for nonlinear SVM using RBF kernel, the penalty parameter,  $C$ , and the kernel parameter,  $\gamma$ , need to be estimated. These parameters determine the capability of the algorithm to separate the hyperplanes. The better these parameters are identified, the more accurate is the prediction of the classifier. The identification of the best  $C$  and  $\gamma$  is performed during the training phase using a cross-validation (CV) procedure, a standard technique to adjust the parameters of prediction algorithms (details of this procedure are shown in Section 3.2). The SVM model, if trained on a large set of “representative” events, can be used to classify any set of data since its training can reach a high level of reliability. The results are used to configure the SVM model. The SVM model retrieved in the previous step is used to classify the whole dataset, providing as output a label for each  $n$ -tuple of input. In this way, a label is associated with each radar sample, providing the spatial distribution of the hydrometeors that build up the weather phenomena occurring in a specific geographical area.

### 3. SVM HCA Validation Using a Simulated Scenario

In general, it is very hard to get appropriate simultaneous measurements for physical validation of HCAs, while the microphysical output of a numerical weather model allows the straightforward evaluation of the capability of the HCA of interpreting the input radar variables to find the most probable hydrometeor class. In this section, the validation of the SVM algorithm using a synthetic set of measurements is shown. After having introduced the weather scenario and the radar simulated variables, the algorithm performances are evaluated in terms of accuracy of the prediction of the hydrometeor classes. First, the ability of SVM to find the correct parameters by varying the size of the training set is presented, then the results of the physical validation based on WRF outputs are shown in terms of confusion matrix.

#### 3.1. Set-Up of a Weather Scenario and Simulation of Radar Observations

The Weather Research and Forecasting model (WRF) is used to provide a set of microphysical descriptors from which the radar observables are extracted. WRF model implementations exist at different temporal and spatial resolution. In this work, the non-hydrostatic model at the horizontal resolution of 1–3 km, able to simulate moist convection and advanced microphysical processes, is used [32]. The WRF loads the General Regularly-distributed Information in Binary form (GRIB) file describing a meteorological event chosen by the user and generates a synthetic 3D scenario providing several meteorological parameters in output (e.g., pressure, wind, temperature, moisture). Using the Millbrandt–Yau two-moment microphysics option [33,34] in WRF, microphysical parameters such as the mixing ratio ( $q$ , in  $\text{kg}\cdot\text{kg}^{-1}$ ), which is the ratio of the water vapor mass to the mass of dry air, and the concentration of particles ( $N_T$ , in  $\text{m}^{-3}$ ), can be obtained. Each microphysical parameter is available for four different classes of hydrometeors: *rain*, *snow*, *graupel*, and *hail*. The WRF outputs are used to generate microphysical parameters and, in combination with the T-matrix code, the corresponding scattering and propagation characteristics are obtained. In particular, in order to set the T-matrix simulation for each hydrometeor class, WRF outputs (wind fields, temperature, and microphysical parameters) have been used to define the size distributions of the particles and the probability density function of the aspect angle and the canting angle. Details on the use of WRF microphysics and additional assumption for running T-matrix are found in [20]. T-matrix provides the covariance matrix of the voltages at the radar receiver for each hydrometeor type from which polarimetric radar parameters can be obtained. Since each element of the WRF volume can contain a

mixture of hydrometeors, the sum of individual voltage covariance matrix of the separate components is calculated [28]. This means that the different types of hydrometeors contribute separately to the covariance matrix, and the contributions of the covariance matrices of the different hydrometeor types can be added together to build the bulk covariance matrix.

A problem in training and testing the HCA using WRF outputs is that there are just four hydrometeor classes available from WRF, while for HCA there are six classes.

In this work, the classes of WRF are determined using the mixing ratio  $q$  in each volume, as shown in Table 1. To obtain the six HCA classes, some were generated by mixing two separate WRF classes. Differences are in the snow class (HCA splits snow in two classes: *wet snow* and *dry snow*), and in the *hail mix* class (this class is present only in HCA and it is a mixture of rain and hail). This classification will be referred to as WRF-class the following.

**Table 1.** Hydrometeor Classification Algorithms (HCA) classes determined by values of  $q$  obtained from the WRF model. The percentages are the mixing ratio quantity of a given hydrometers with respect to the sum of  $q$  of all classes. DS stand for *dry snow*, WS for *wet snow*, and HM for *hail mix*. For instance, the rain class is defined when the percentage of  $q_{rain}$  is greater than 90%, while WS class is defined when  $q_{rain}$  is greater than 30% and  $q_{snow}$  is greater than 60%.

	Rain	DS	WS	Graupel	Hail	HM
$q_{rain}$	>90%	0	>30%	0	0	>30%
$q_{snow}$	0	>90%	>60%	0	0	0
$q_{graup}$	0	0		>90%	0	
$q_{hail}$	0	0		0	>90%	>60%

The intense precipitation event that occurred on the afternoon of 15 October 2012 in the Southern Mediterranean and off the coast of Tunisia is selected as the test case to run the WRF model. The WRF scenario selected is composed of a cubic volume of  $800 \times 682 \times 52$  elements, whose resolution is  $300 \text{ m} \times 300 \text{ m} \times 150 \text{ m}$ , the last being the vertical resolution. WRF provides for each element of the cube and for each hydrometeor class the microphysical characteristics ( $q$  and  $N_T$ ), and the meteorological variables (pressure, temperature, wind speed, and direction). Using the T-matrix code, the polarimetric radar parameters are calculated for each element of the WRF scenario. The polarimetric parameters obtained in this way are ideal values. In order to generate realistic polarimetric variables as would be measured by a real radar system, an error term simulating the effect of signal fluctuations is added. A radar system with a three-degree antenna beamwidth (a typical aperture of radar antennas mounted on civil aircrafts), operating at a frequency of 9.353 GHz, with a range resolution of 150 m has been assumed. Then, Gaussian distributed random variables have been added to ideal radar parameters obtained by WRF output. The standard deviations are set to 1 dB for  $Z_h$ , 0.2 dB for  $Z_{dr}$  and 0.01 for  $\rho_{hv}$ , while the  $K_{dp}$  standard deviation is calculated using the following formula [28]:

$$\sigma(K_{dp}) = \frac{\sigma(\Phi_{dp})}{L} \sqrt{\frac{3}{\left[N - \left(\frac{1}{N}\right)\right]}} \quad (1)$$

where  $\sigma(\Phi_{dp})$  is the standard deviation of  $\Phi_{dp}$ , fixed at  $5^\circ$ ,  $L$  is the path length along which derivative estimation is performed, fixed at 1.5 km, and  $N$  is the number of range bins that are 10 in this case. The resulting value of  $\sigma(K_{dp})$  is approximately  $0.1^\circ \text{ km}^{-1}$ .

### 3.2. SVM Parameters Optimization

A SVM HCA algorithm has been implemented for the WRF scenario using realistic radar measurements (with noise added) and the height of  $0^\circ \text{C}$  level given by the WRF model. The training set is obtained random sampling the elements of the volume of data and includes  $10^5$  samples, while a test set of  $3 \times 10^6$  samples (randomly sampled and excluding the samples belonging to the training

set) was used to test the classifier. In order to get an estimate of SVM algorithm accuracy on predicting the membership functions of a certain class, typical steps are: (i) finding optimal tuning parameters; (ii) training a model using these optimal parameters on the full training set and (iii) testing this model on the test set. For the SVM scheme used in this work (with RBF kernel) the values of  $C$  and  $\gamma$  (see Section 2.1) need to be identified. It is not known beforehand which are the best values of  $C$  and  $\gamma$  for a given problem. A cross-validation procedure is used to get an accurate idea of the generalization error when certain tuning parameters are used, and an accurate CV can prevent the overfitting. A “grid-search” on  $C$  and  $\gamma$  using CV is performed: different pairs of  $(C, \gamma)$  values are tried and the one with the best CV accuracy is picked. To identify good parameters, a useful method is to try exponentially growing sequences of  $C$  and  $\gamma$ . Figure 1 shows the final grid plot of the grid-search process, in which a 94.8% accuracy was found for this SVM model for the best values  $C = 8$  and  $\gamma = 2$ . In order to find how large the training set selected should be to achieve the desired degree of accuracy of prediction, the CV is performed at different size of the training set that varied from  $10^2$  up to  $10^5$ . Figure 2 shows that larger training subsets increase the CV accuracy, but also that when a certain size (in this case  $10^4$ ) is exceeded, the CV accuracy does not increase significantly (the CV increase from  $10^4$  to  $10^5$  is around 1%): therefore, when this size is reached the code can be stopped. These processes demonstrate that  $10^4$  observations are sufficient to train the SVM model with a high accuracy (94.8%) and in a reasonable processing time (less than 1 minute on an x86\_64 Linux machine Eight core, Intel-i7@2,80GHz processor).

CV accuracy is a good measurement to optimize a SVM algorithm, but it does not allow us to evaluate whether all the classes in the training set are well represented by the SV. In fact, when the training is performed using random sampling, the classes that have low occurrences could not be sampled enough to establish a robust relationship. In order to allow adequate representation of all the classes in the model, the training set is quasi-equally divided among the classes. To assume such equiprobability of classes, the training set should be partitioned equally in to six classes. In this work, the maximum number of elements of the less numerous class is used to limit the number of element of each class that composed the training set.

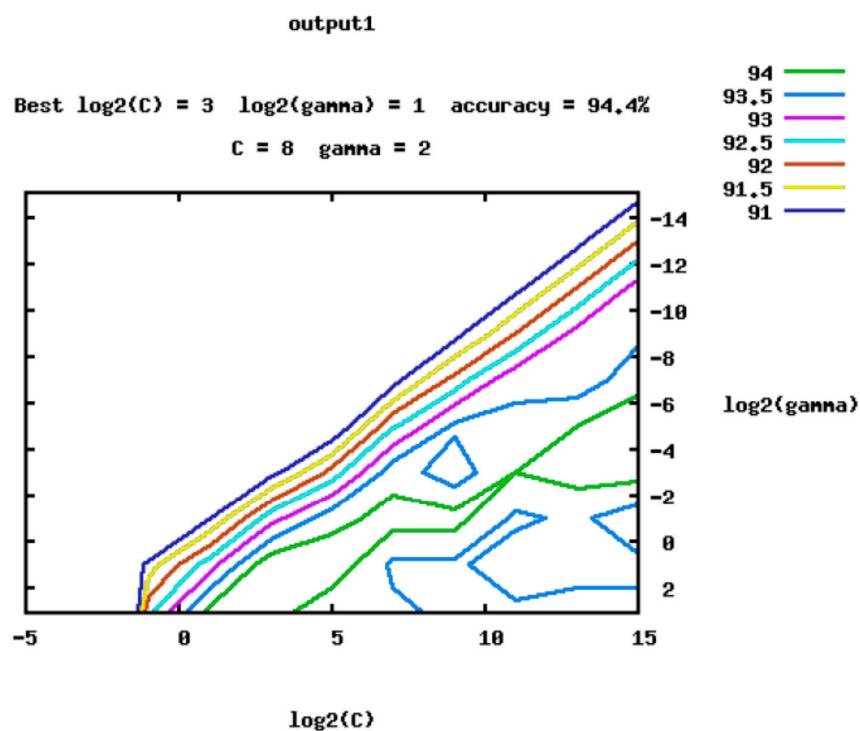


**Figure 1.** Example of parameter estimation ( $C$  and  $\gamma$ ) using a grid search process during the cross-validation.



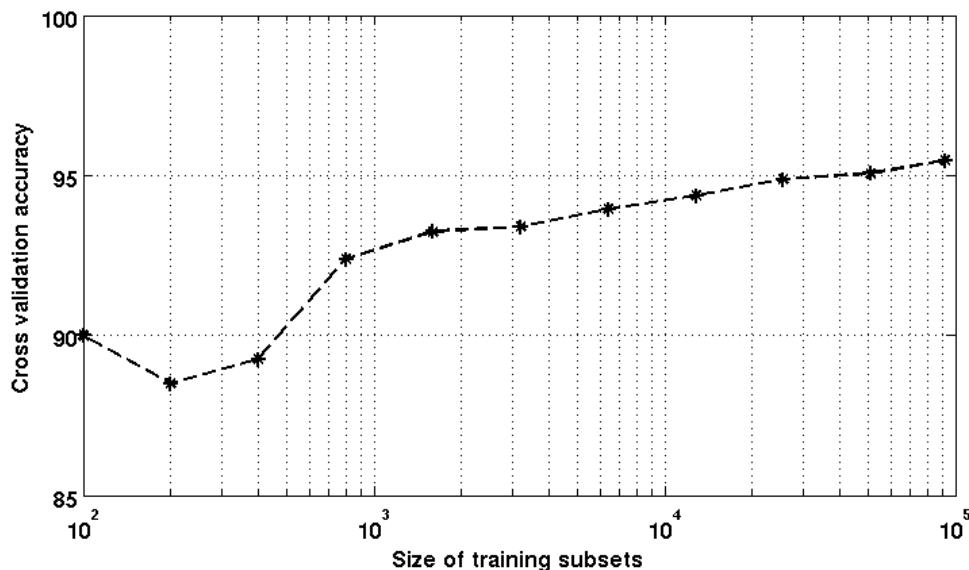


**Figure 2.** The cross-validation accuracy (in percentage) versus the size of the training subsets.

### 3.3. SVM HCA Validation Using WRF Model Output

In addition to the performance of the SVM in separating hyperplanes, i.e., in finding the optimal parameters, we have also evaluated the classification results in terms of ability to identify hydrometeor classes. The validation of the classes predicted by the SVM with respect to the WRF microphysics expressed in terms of the  $q$  parameter (WRF-class) has been performed through the following method. The confusion matrix (CM) has been calculated between the truth and the predicted hydrometeor classes applied at the same test set. The element  $CM(i, j)$  contains the number of observations classified in the  $i$ th class, which in reality belong to the  $j$ th class. The diagonal contains the same classification for both algorithms (correct classification). Given the CM, the global performance of the SVM is quantified by the overall accuracy (OA), defined as

$$OA = \frac{\sum_{i=1}^L CM(i, i)}{m} \times 100 \quad (2)$$

and the Cohen's Kappa (K),

$$K = \frac{OA - P_e}{1 - P_e} \quad (3)$$

where

$$P_e = \frac{\sum_{i=1}^L (\sum_{j=1}^L CM_{j,i} \sum_{j=1}^L CM_{i,j})}{m^2} \quad (4)$$

where  $L$  is the total number of classes ( $L = 6$ ) and  $m$  is the total number of observations.  $K$  takes into account the correct predictions that might occur by chance ( $P_e$ ) and is a robust metric in the case of unbalanced classes.

In this study, the six classes of WRF-class are used to build up the microphysical validation set. The WRF scenario contains  $2.8 \times 10^7$  samples, each one associated to a vector of five elements (radar measurements and height), which implies a huge amount of data to be processed. In order to reduce the number of samples to be processed, and consequently, to reduce the computation time,  $2 \times 10^5$  elements are randomly extracted from the WRF cubic volume. A Monte Carlo method is applied to each sample of the subset in order to generate 100 sets of polarimetric variables, randomly extracting 100 realizations of a set of radar realistic variables and generating a dataset of  $100 \times 2 \times 10^5$  samples. The dataset obtained by the Monte Carlo method is then used to implement the SVM model, splitting it in two sub-datasets, one for training (by extracting  $10^4$  samples and respecting

the equal distribution of samples among the six classes) and the other (consisting of the samples left) for testing. The SVM classification is applied to each set of random variables generating a synthetic dataset of 100 realizations. These synthetic scenarios allow us to estimate the confidence intervals (CIs, namely the 10th and 90th percentile) of the established metrics, calculating for each realization the CM and the respective OA and K coefficients. The CM with the CIs intervals is shown in Table 2. Main differences are found for *wet snow* and *hail mix*, that are additional to the four default classes of the WRF model. The *wet snow* class of WRF is distributed between *rain*, *dry snow*, *wet snow* and *graupel*, of SVM classes; the *hail* class of WRF is mostly associated with the *hail mix* of SVM class. Details on the radar dual-polarization signatures of WRF-class classes comparing to HCA classes are presented in Appendix B.

**Table 2.** Confusion matrix per class of the WRF scenario obtained by using  $100 \times 2 \times 10^5$  observations for each realization (infinite values are excluded in the CM). For each element, the CIs intervals (found using, the 10th, 50th, and 90th percentiles) are shown. Classifications matched by WRF and SVM are found along the diagonal and misclassifications are in the off-diagonal entries.

		<i>Model (WRF)</i>					
		<b>Rain</b>	<b>DS</b>	<b>WS</b>	<b>Graupel</b>	<b>Hail</b>	<b>HM</b>
<i>Predicted (SVM)</i>	<b>Rain</b>	51,390.0	1252.5	6289.0	567.0	210.0	913.5
		<b>51,447.0</b>	<b>1275.0</b>	<b>6320.0</b>	<b>592.5</b>	<b>222.0</b>	<b>941.0</b>
		51,511.0	1290.0	6351.0	610.5	231.5	967.0
	<b>DS</b>	823.0	41,477.5	9689.0	5136.0	6.0	6.0
		<b>835.5</b>	<b>41,524.0</b>	<b>9702.5</b>	<b>5172.0</b>	<b>8.0</b>	<b>7.0</b>
		852.0	41,585.5	9714.5	5209.0	10.0	9.0
	<b>WS</b>	902.0	1940.0	2308.0	2382.0	13.0	172.0
		<b>917.0</b>	<b>1964.0</b>	<b>2327.0</b>	<b>2422.5</b>	<b>16.0</b>	<b>180.0</b>
		935.5	1993.0	2345.0	2454.5	20.0	190.0
	<b>Graupel</b>	4566.5	7401.5	916.5	17,119.0	2.0	17.0
		<b>4601.0</b>	<b>7457.5</b>	<b>951.0</b>	<b>17,168.5</b>	<b>4.0</b>	<b>22.0</b>
		4648.5	7515.5	980.5	17,219.5	6.0	27.0
	<b>Hail</b>	1087.0	0.0	0.0	48.5.0	1311.0	1627.5
		<b>1112.5</b>	<b>0.0</b>	<b>0.0</b>	<b>56.5</b>	<b>1352.5</b>	<b>1668.0</b>
		1151.0	0.0	0.0	67.0	1407.0	1719.0
	<b>HM</b>	7059.5	0.0	0.0	124.5	16,346.0	16,029.0
		<b>7106.5</b>	<b>0.0</b>	<b>0.0</b>	<b>135.0</b>	<b>16,396.0</b>	<b>16,082.5</b>
		7144.5	0.0	1.0	147.0	16,443.0	16,120.0

In spite of the differences between the WRF and SVM classes, good performances are obtained for SVM classifications using the metric described above and calculating the respective CIs. The CI found for the OA is [64.89 **64.95** 65.02]% and for the K is [0.5506 **0.5513** 0.5522]. CIs are very narrow, meaning that measurement errors do not impact on classification results. Moreover, results obtained from the comparison between WRF microphysics and SVM HCA using CM highlight that SVM model gives a fairly good prediction of WRF classes via the FL training set. More results relative to SVM classification performance are shown in Section 4, describing the behavior of the SVM HCA applied to real datasets.

The structure of the SVM is easily reconfigurable: it possible to train the algorithm using any type of adequate validation dataset available. For hydrometeor classification purposes, different data sources can be investigated to train the algorithm, such as different Numerical Weather Prediction model outputs or other sensor information, e.g., disdrometer measurements [15].

#### 4. Evaluation of the SVM Hydrometeor Classification with Real Measurements

The SVM model presented in Section 2 has been applied to measurements collected by X- and C-band ground based systems. Two datasets have been analyzed: one includes measurements collected on 2013 by an X-band dual-polarization Doppler radar operating within Catania airport, and the other includes measurements collected on 2012 and 2015 by the Polar 55 C, C-band dual-polarization Doppler located in Rome. The training phase was implemented with the support of the fuzzy logic classification scheme according to the approach explained in Section 2.2.

##### 4.1. C-Band Dataset

Sixteen intense precipitation events that occurred over Central Italy in September–October 2012 during the Special Observation Period 1 (SOP1) of the Hydrological cycle in Mediterranean Experiment (HyMeX) and an event that occurred on 12 October 2015 [9,35] were selected to evaluate the SVM HCA algorithm. Although these events have predominantly convective characteristics, they include parts during which the precipitation was less intense and exhibit stratiform characteristics. These events were observed by the Polar 55C radar located in Rome (latitude: 41.842° N, longitude: 12.646° E, 132 m above sea level) at ISAC-CNR. Polar 55C is a research-grade C-band (5.6 GHz frequency) Doppler dual polarization radar (details of the system characteristics can be found in [36]). The data selected were collected with a volume scanning composed of 7 or 8 Plane Position Indicator (PPI) at different elevations (from 0.6° to 12°) performed every 5 min. In addition, some sweeps along the vertical were performed for  $Z_{dr}$  calibration and for detailing the vertical structure of precipitation. Moreover, sweeps at fixed azimuths with varying elevation (Range Height Indicator, RHI) were also performed to scan the most intense convective cells. The range resolution was 75 m, corresponding to a pulse duration of 0.5  $\mu$ s. The pulse repetition frequency was 1200 Hz while the maximum range was limited to 120 km. To test the classification performance, the SVM HCA was applied to all the volume scans (in total 1257 volumes consisting of 7–8 PPIs depending on the case study) and the 33 RHI scans (in each map  $360 \times 1600$  samples). Data were corrected for attenuation due to propagation as described in Section 2.2. The training set was obtained by a random selection of 100 volumes classified by the FL scheme that contains different type of precipitation regimes (convective and stratiform). After the random selection, a human inspection on the 100 volumes was made in order to check that these volumes include both convective and stratiform precipitation regimes (at least 20% and 80%). Finally, from these datasets  $10^4$  samples (not empty) were randomly extracted (respecting the equipartition of sampled per the class) to build the training set.

##### 4.2. X-Band Dataset

The case studies considered occurred on 21 February and 21 August 2013 in Sicily and were observed by the Selex-Gematronik 50 DX system (with a 3 dB antenna beamwidth of 1.3° and a transmit peak power of 50 kW) of the Department of Civil Protection of Italy, operational at the airport of Catania [27]. The radar performed a volume scan made of 12 sweeps at different antenna elevation angles ranging from 1° to 21.6°, and an additional one at vertical incidence. The range resolution was 200 m and the maximum unambiguous range was 80 km, corresponding to a PRF of 1875 Hz. The dataset consists of 19 volumes collected during the intense part of the 21 February event and 55 volumes during the 21 August 2013 event. Each radar volume contains  $1.7 \times 10^6$  samples. As demonstrated in Section 3.2,  $10^4$  samples are sufficient to train the SVM model. Ten radar volumes among the 74 available were selected for the training phase (and excluded from the test set), from which a subset of  $10^4$  samples was obtained by a random selection respecting the equipartition of samples per class.

### 4.3. Comparison of Results from SVM and FL Classification

In order to evaluate the performance of SVM model with real data, qualitative and quantitative comparisons with output provided by the FL classification are discussed in this section. SVM classification results applied to Polar 55C quasi-horizontal sweeps are shown in Figures 3 and 4 for two volumes collected on 15 October 2012 and 12 October 2015 during intense precipitation. Upper panels show a PPI presentation of the classification results pertinent to data collected at  $1.6^\circ$  elevation, while bottom panels show the pseudo RHI reconstructed from volume data along specific rays. The output of the SVM (panels in left column) is compared, for the same data, with the output of the FL classifier (panels in right column). At first glance, the results do not differ much from each other, as expected. However, it can be noticed that the SVM classifier is able to classify data that are not classified (labeled as “None” and plotted in gray) by the FL classifier. In fact, the last stage of FL process consists in assigning a class based on rule strength. If it falls below a certain threshold [28], a pixel is labeled as not classified, while the SVM model always assigns a class label to a set of radar measurements. Furthermore, the SVM output appears more homogeneous and less noisy than the FL output. For example, the graupel area detected by the SVM shown on the pseudo RHI of Figure 3 (left panel) is less fragmented than the corresponding area classified by the FL (right panel). Nevertheless, since both classification approaches are applied on a point-by-point basis, such results can be attributed to the ability of SVM to learn from the entire hyperspace of radar measurements and to the accurate training of the model that includes high number of maps used (i.e., each class is assigned by SVM HCA based on relations obtained combining in several ways polarimetric radar variable). More impressive is the performance of SVM applied to the data shown in the RHI plots of Figure 5, where spatial homogeneity and spatial coherence are more evident with respect to the classification map obtained with the FL. Two convective cells are well distinguished, the first one close to the radar (at less than 20 km) and extended up to 8 km height, and the other one at around 50 km of distance, reaching 5 km height. Both cells are characterized by a core of graupel and rain close to ground, but the SVM classifier (upper panel) well identifies these cells detecting homogenous graupel region, while the FL classification (bottom panel) of these cells is fragmented in non-identified and spurious hydrometeors types. Figures 6 and 7 show the pseudo-RHI for the two X-band case studies classified using SVM model (Figures 6a and 7a) and FL schemes (Figures 6b and 7b). Even at X-band, it can be noticed that the SVM classification results appear more spatially homogeneous in terms of image texture.

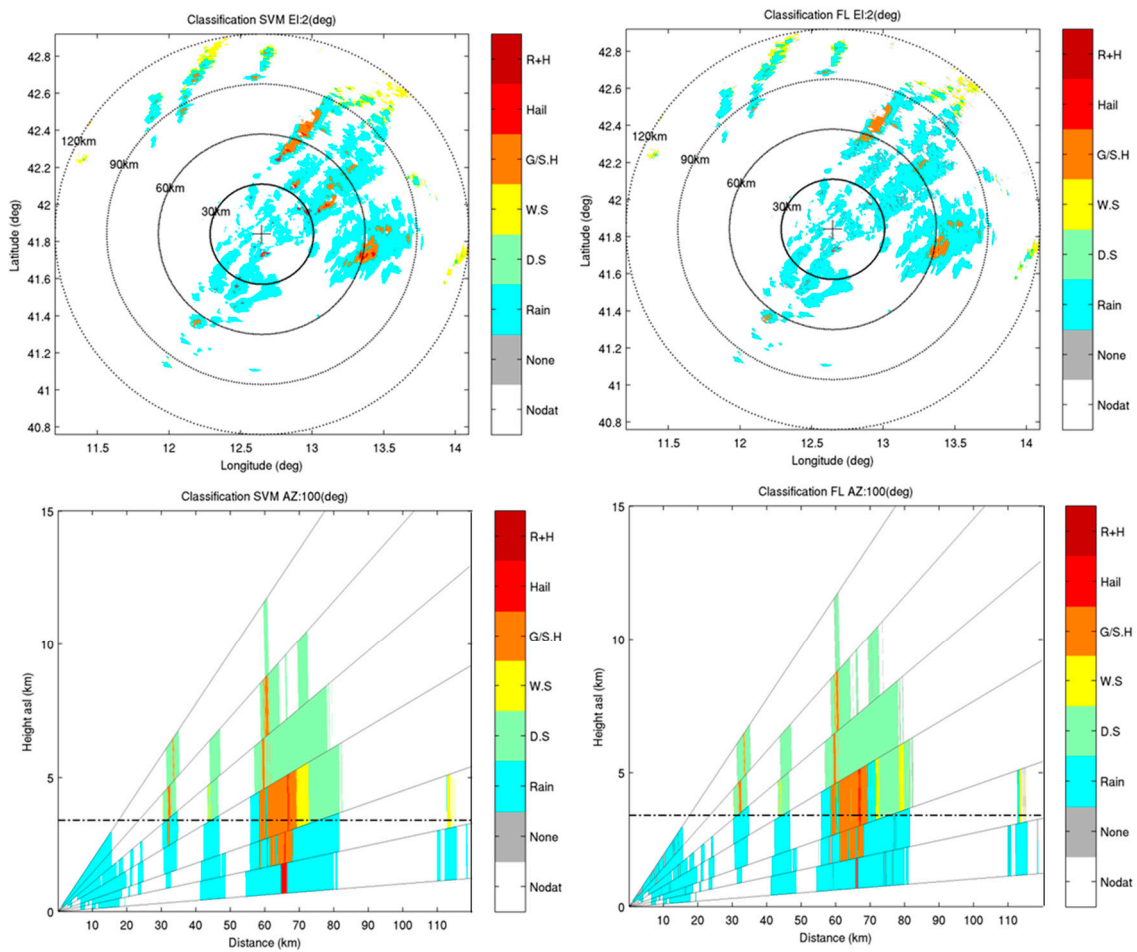


**Figure 3.** Hydrometeor classification applied to the volume collected on 15 October 2012 at 1016 UTC by the Polar 55C radar. Left column: Support Vector Machine (SVM) approach results; Right column: FL approach results. Upper panels show the Plane Position Indicator (PPI) at  $1.6^\circ$  and the bottom panels show the pseudo Range Height Indicator (RHI) at  $100^\circ$  azimuth. In the legend of this and of the following figures “R+H” stands for *hail mix*; “G/S:H” stands for *graupel*; “WS” stands for *wet snow*; “DS” stands for *dry snow*; “none” stands for *not classified*; “nodat” stands for *no data*.



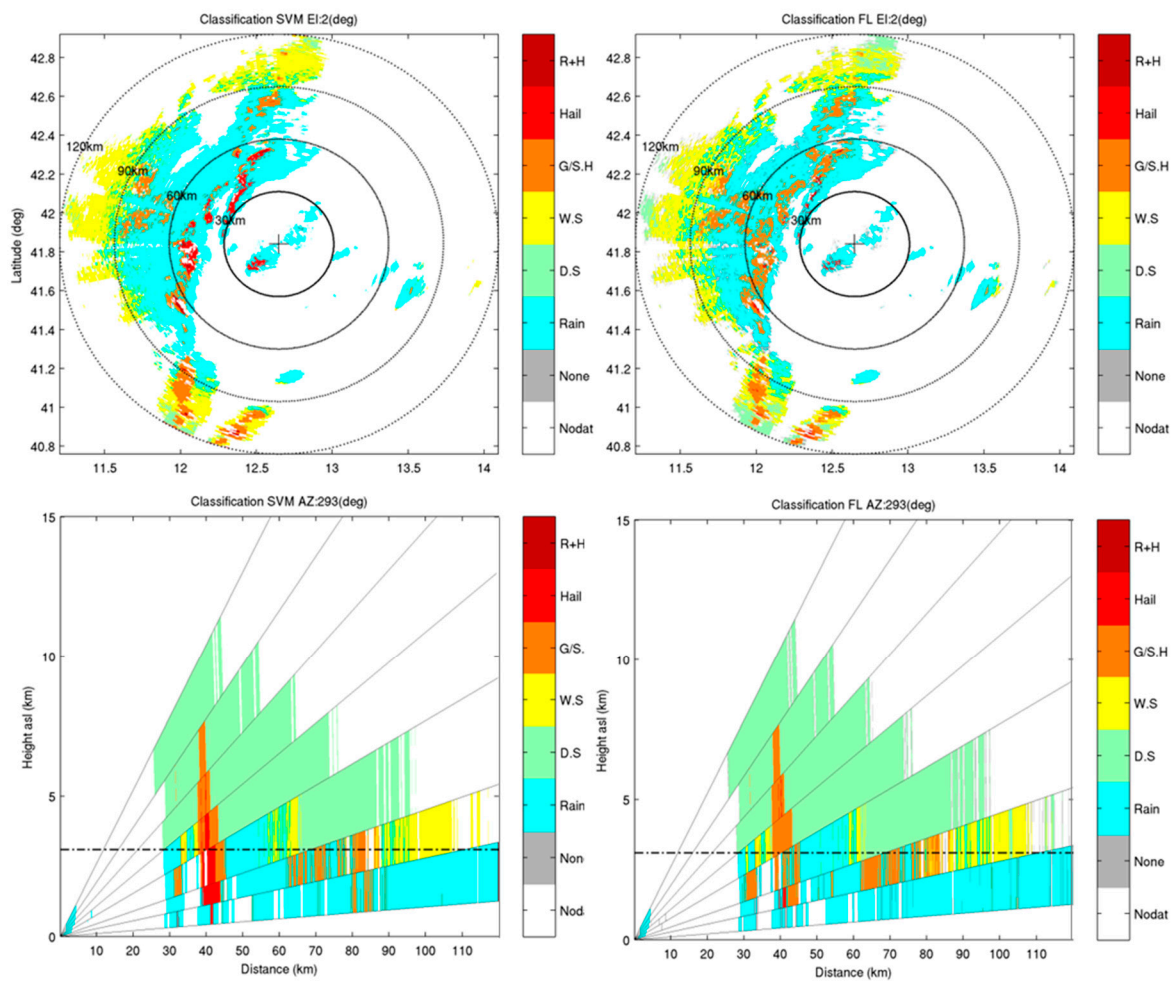


**Figure 4.** Hydrometeor classification applied to 12 October 2015 at 1305 UTC case study: SVM approach in first column and FL in second column. Upper panels show the PPI at  $1.6^\circ$  and bottom panels show the pseudo RHI for  $66^\circ$  azimuth.

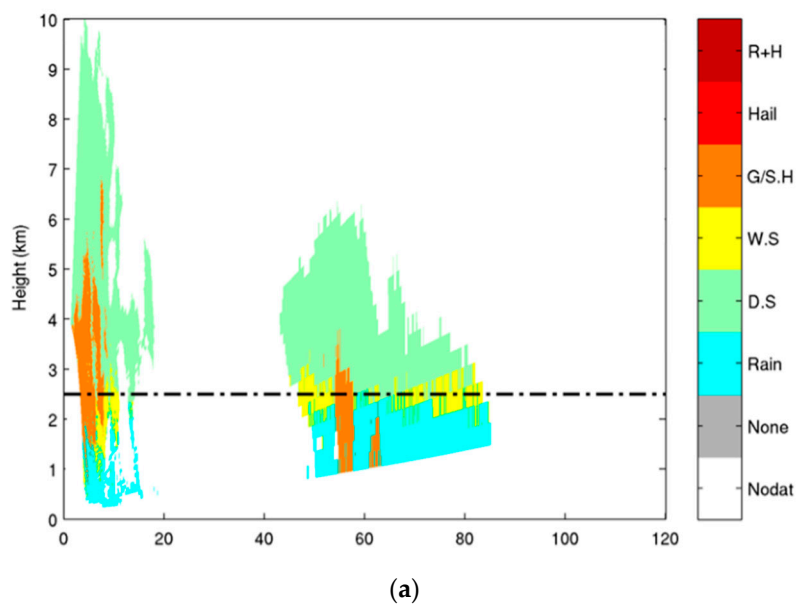


**Figure 5.** Cont.

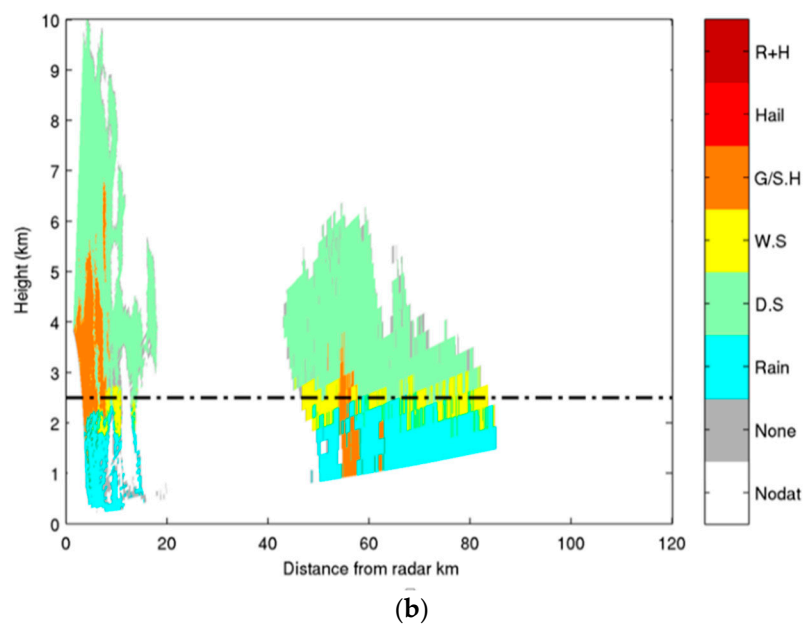


**Figure 5.** RHI sweep performed by Polar 55C on 15 October 2012 at 1738 UTC (293° azimuth) classified by SVM (a) and FL (b).

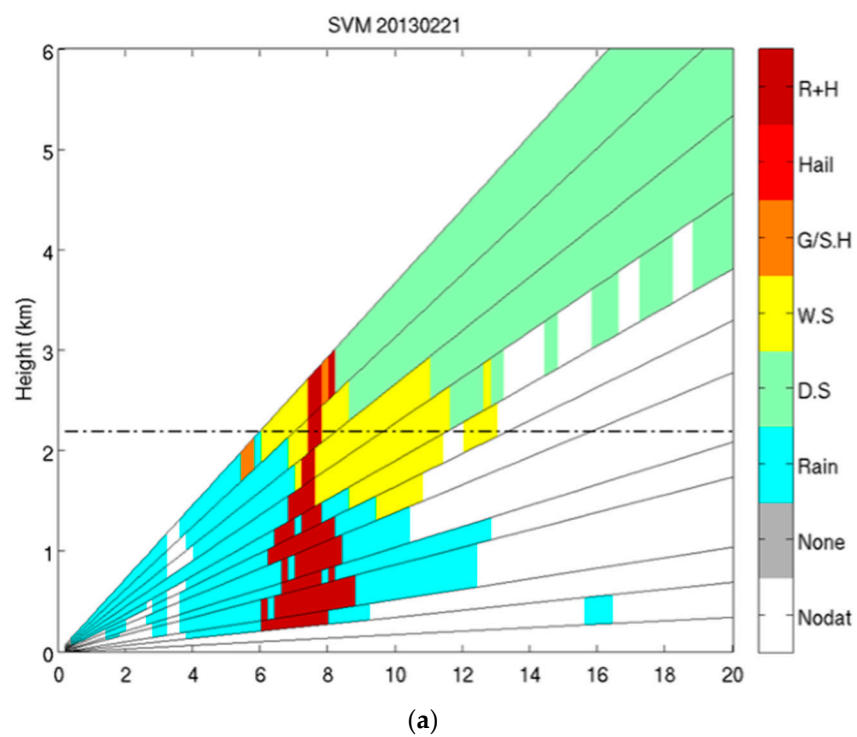


**Figure 6.** *Cont.*

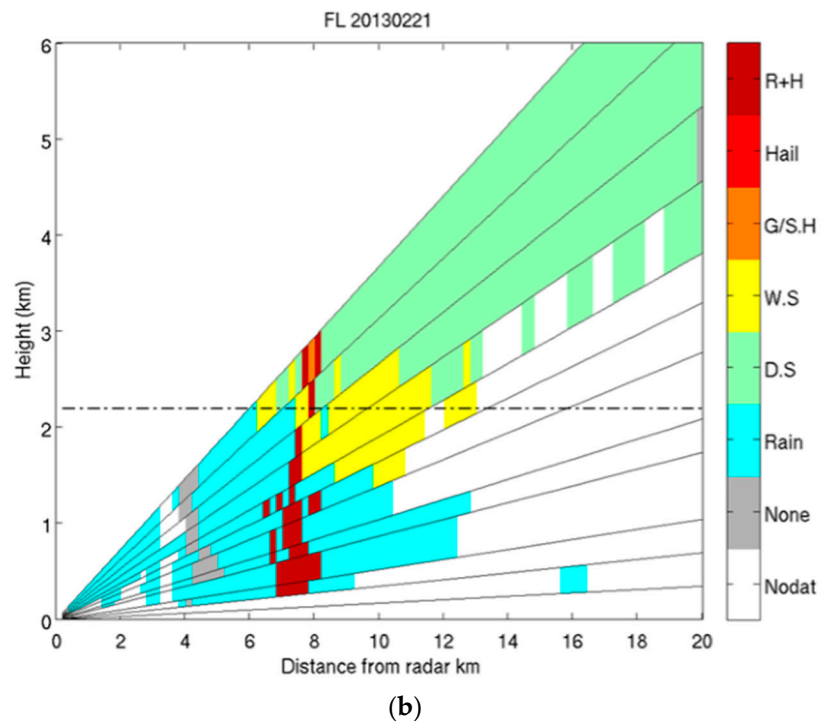


**Figure 6.** Vertical cut of SVM classification (a) and FL classification (b) applied to data gathered by the X-band radar at 4° azimuth on 21 February 2013 at 1520 UTC.

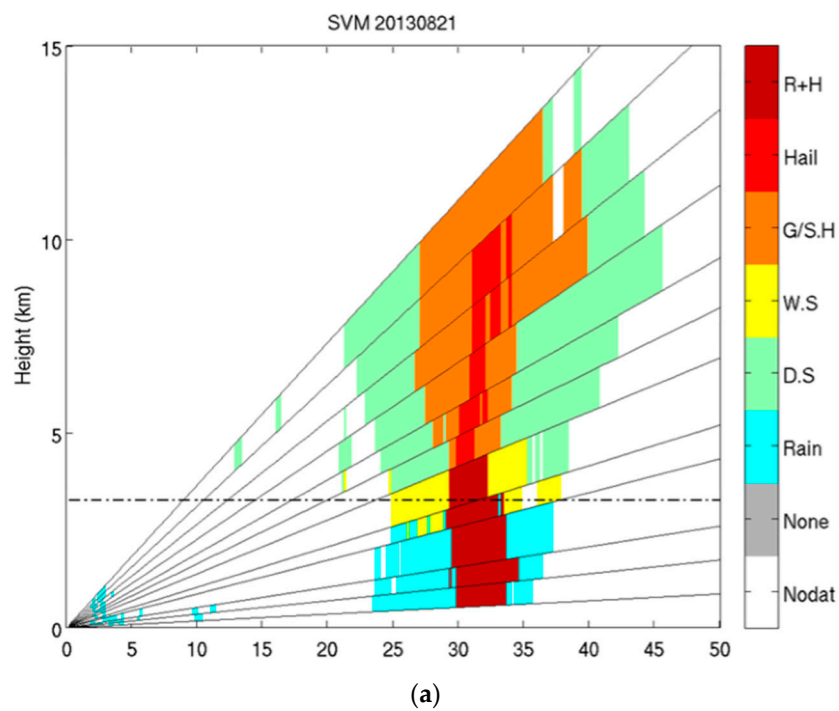


**Figure 7.** Cont.

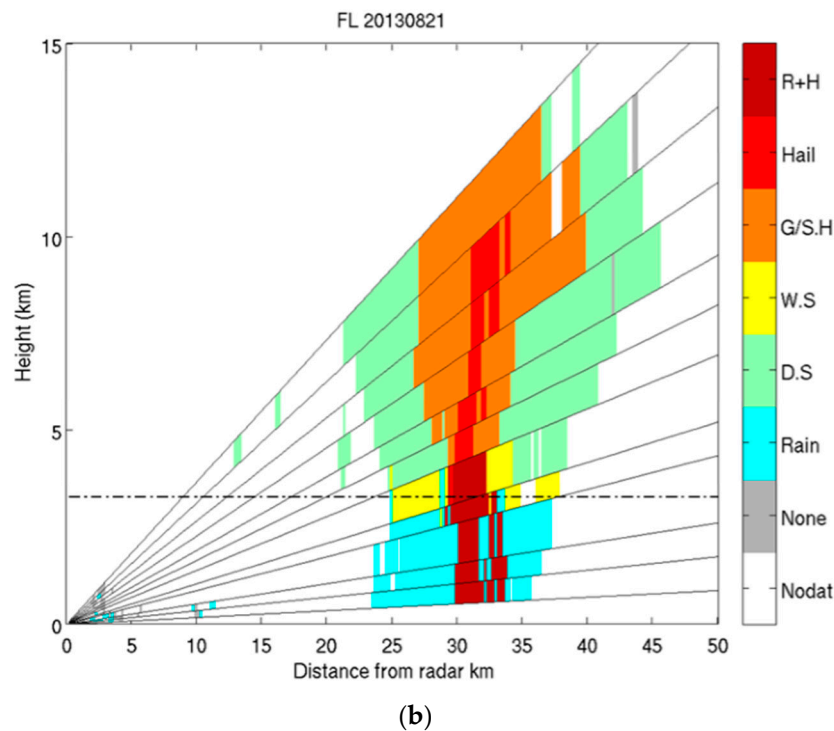


**Figure 7.** As in of Figure 6, vertical cuts for SVM and FL classifications applied to data gathered at 122° azimuth on 21 August 2013 at 0450 UTC.

Besides the qualitative comparison between classification maps, the SVM model performance can be objectively evaluated with respect to the FL classification. Since a “true” reference is not available, some quantitative indicators must be used. A number of quantitative indices have been calculated, such as texture image parameters, connected component labeling (CCN), and labels classified by SVM respect to unclassified by FL. The following parameters have been evaluated from the co-occurrence matrix considering horizontal neighboring resolution cell separated by distance 1, as illustrated in [37]:

$$Co(i, j) = \sum_m \sum_n \begin{cases} 1, & \text{if } I(m, n \pm 1) = i \text{ and } I(m, n) = j \\ 0, & \text{otherwise} \end{cases} \quad (5)$$

where  $m, n$  are the position indices and  $i, j$  are the indices of the class values (from 1 to 6). The normalized co-occurrence matrix,  $N_d(i, j)$  is obtained dividing the  $Co$  matrix by the sum of its elements  $\sum_n \sum_m Co(n, m)$ . From  $N_d$  are derived:

$$Energy = \sum_i \sum_j N_d^2(i, j) \quad (6)$$

$$Entropy = - \sum_i \sum_j N_d(i, j) \log_2 N_d(i, j) \quad (7)$$

$$Homogeneity = \sum_i \sum_j \frac{N_d(i, j)}{1 + |i - j|} \quad (8)$$

These features are frequently used to characterize images. Energy measures the textural uniformity, i.e., pixel pairs’ repetition, by detecting disorders in textures. High energy values occur when the class distribution has a periodic pattern. The entropy is a feature that measures the randomness of class distribution. The entropy is large when the image is not texturally uniform and  $Co$  matrix elements have very small values. Complex textures tend to have high entropy. Entropy

is strongly, but inversely, correlated to energy. Homogeneity measures image homogeneity as it assumes larger values for small differences in pair elements. It is more sensitive to the presence of near diagonal elements in the  $C_o$  matrix. It is at a maximum when all elements in the image are identical. In this work these indices are compared one to one for the same image in order to get information on possible improvement of SVM classifications in term of hydrometeor spatial coherence with respect to the FL classification. Energy and homogeneity are features that measure the uniformity of class distribution and their values are expected to be high. The spatial homogeneity is also assessed by the CCN technique. Given a map the number of connected region  $N_r(k)$ , where  $k$  is the class label, are identified by the CCL algorithm [38] checking eight connections and the regions are sequentially labeled. A hydrometeor class can be considered spatially homogeneous when the CCL algorithm detects a low number of  $N_r(k)$  for that class. In this metric, when the two classification maps (SVM and FL) for the same scene are compared, the one that presents the smallest number of CCL, calculated by the index  $S = \sum_k N_r(k)$ , is the one with the highest spatial homogeneity. Quantitative indices are calculated for corresponding classification map pairs.

Since RHI maps at C-band and volumes of PPI at X-band are of the order of tens, quantitative indices are calculated for selected maps. The SVM classification for the RHI map (upper panel in Figure 5) is clearly spatial homogenous and coherent with respect to the FL classification. These qualitative considerations are confirmed by good performances obtained by the quantitative indices listed in Table 3. Quantitative indices for classification results obtained by the SVM and FL HCAs. Scores are referred to the C-band RHI shown in Figure 5. Major improvements are registered in terms of homogeneity and energy, while entropy does not vary. Despite the high number of CCL found in this scene, there are 42 CCL less in the SVM classification map than in the FL one and 2404 pixels not classified in the FL classification map are instead labeled by the SVM HCA. X-band scores related to the SVM classification for the two scenes shown in Figures 6 and 7, exhibit slight improvements on all indices compared to the scores related to the FL classification (Table 4).

**Table 3.** Quantitative indices for classification results obtained by the SVM and FL HCAs. Scores are referred to the C-band RHI shown in Figure 5.

	None	Energy	Entropy	Homogeneity	S
<i>20121015 1738UTC</i>					
<b>SVM</b>	0	0.424	0.369	0.957	281
<b>FL</b>	2404	0.341	0.365	0.893	323

**Table 4.** As in Table 3, scores refer to two X-band classification maps shown in Figure 6 (upper lines) and Figure 7 (lower lines).

	None	Energy	Entropy	Homogeneity	S
<i>20130821 0450UTC</i>					
<b>SVM</b>	0	0.255	0.951	0.977	29
<b>FL</b>	73	0.247	0.939	0.958	37
<i>20130221 1520UTC</i>					
<b>SVM</b>	0	0.333	0.689	0.952	17
<b>FL</b>	24	0.336	0.678	0.937	19

The number of test maps available for C-band is 1257, considering all the PPI scans in the volumes for all the case studies. In order to obtain a consistent statistical sample, 100 pairs of maps have been randomly extracted (without replacing samples) and the quantitative indices calculated comparing each couple of maps. Table 5 shows the CIs for each quantitative index, calculating the 10th, 50th, and



90th percentiles. The SVM classification exhibits good performances for all indices with respect to the FL classification. Noticeable are homogeneity scores: the SVM values are very close to one (the lower limit of CIs is 0.93 and the upper limit is 0.99). Furthermore, an index of low fragmentation texture of the maps is found in the SVM classification, where they exhibit a smaller CCL (448.5 at 50th percentile) with respect to the FL maps (473.5 at 50th percentile). Finally, 3062.5 non-classified pixels are found at 50th percentile in the FL classification maps, which are instead assigned in the SVM classification maps.

**Table 5.** Quantitative indices for classification results obtained by the SVM and FL HCA. The dataset consists of 100 PPIs collected by Polar 55C at 1.6° elevation angle extracted randomly from the entire dataset. The CIs for each index are derived from the 10th, 50th, and 90th percentiles are listed for each classification approach.

	None	Energy	Entropy	Homogeneity	S
SVM	0	0.645	0.105	0.933	87
	<b>0</b>	<b>0.820</b>	<b>0.339</b>	<b>0.964</b>	<b>448.5</b>
	0	0.981	0.784	0.996	1691.5
FL	900.5	0.414	0.102	0.790	77.5
	<b>3062.5</b>	<b>0.663</b>	<b>0.334</b>	<b>0.861</b>	<b>473.5</b>
	9527.5	0.790	0.776	0.917	2126

## 5. Conclusions

A supervised hydrometeor classification approach based on a learning machine method, a Support Vector Machine, is presented in this work. The algorithm, after having established robust relations between input variables and known samples (training phase), is able to predict the membership class of an unknown sample (prediction phase). Input variables are four dual-polarization radar measurements and the height of the 0 °C level. Results obtained by a fuzzy logic HCA, one of the most used hydrometeor classification approaches based on empirical rules, have been used as reference to train the SVM algorithm. The challenging task of validation has been achieved with realistic scenarios generated by the numerical weather prediction model WRF. Validation skills in hydrometeor identification of the SVM algorithm have been evaluated by using the output of the WRF model in which microphysical scheme are explicit. Hydrometeor classification has been performed in each grid point of WRF in which microphysics characteristics, denoted by mixing ratio for four hydrometeor class, were known. Six hydrometeor classes that include two additional classes with respect to WRF scheme (obtained by mixing two classes) have been derived by quantifying the mixing ratio. From the WRF model outputs, realistic polarimetric radar measurements were simulated by using the T-matrix code and adding random errors to each radar variable. The HCA-SVM classification and the WRF outputs were compared (on  $2 \times 10^5$  samples of the WRF scenario) by calculating a confusion matrix matching the six hydrometeor classes: good performances were obtained finding 65% of overall accuracy and 0.55 of Cohen's coefficient.

The HCA algorithm has also been applied to real radar measurements collected by two ground based radar systems at X- and C-band. Two case studies occurred during 2015 in Sicily were observed by the X-band dual polarization Doppler radar located at Catania's airport, while several observations were made in Central Italy during 2012 and 2015 by the C-band dual-polarization Doppler radar located in Rome at ISAC. Data collected using scanning modes (PPI volumes and RHI) were included in the dataset. The SVM algorithm has been trained by randomly sampling a part of the dataset and the rest part was used as test. To evaluate the SVM classification results, operational classification product obtained by using the FL approach has been applied to the same dataset. Qualitative comparisons between FL and SVM classification maps have revealed several positive features of the SVM classifier: (i) the texture of the maps is more homogeneous and less noisy; (ii) the maps appear more spatially coherent and homogeneous; and (iii) pixels not classified by the FL classification are classified by the SVM in a manner that appears consistent with the classes of the neighboring pixels. In order to quantify

these SVM skills, some quantitative indices, mainly related to textural analysis, have been calculated for each pair of classification maps. Such a quantitative analysis has confirmed the benefits conferred by the SVM classification. In particular, RHIs classification maps have shown the highest scores: energy and homogeneity have increased of 20% and 10%, respectively, and more than 2400 not classified pixels have been assigned to a hydrometeor class by SVM HCA. Thanks to a large availability of PPI volumes at C-band (1257 volumes), a dataset of 100 maps has been selected and quantitative indices calculated at the 10th, 50th, and 90th percentiles. Indices related to texture analysis of image, energy and homogeneity, increased around 21% and around 12% (at the 50th percentile), respectively. The improvements found by SVM classifier with respect to FL, even though both classification approaches are applied pixel-by-pixel, can be attributed: (i) to thousands of pixels classified by SVM (not classified in FL); (ii) to the ability of SVM to learn from the entire hyperspace of radar measurements and (iii) to the accurate training of the model, which includes a large number of maps.

Besides the good performance of SVM in terms of hydrometeor identification shown in this work, the SVM approach has also exhibited a superior computational efficiency with respect to the FL approach. This suggests the possibility of using the SVM HCA in quasi-real-time tasks, as could be required by avionic applications running on devices that process radar measurements collected during the flight, with the purpose of avoiding areas characterized by hazardous weather.

**Acknowledgments:** The authors acknowledge the support of the European Union Clean Sky Joint Technology Initiative, activity “System for Green Operation” through the projects KLEAN (Project ID: 306927), X-Wald (Project ID: 619236), and Win-FC (Project ID: 632536). Authors thank the Department of Civil Protection of Italy for providing X-band radar data. Content of this paper reflects only the authors’ views. Clean Sky JU and European Union are not liable for any use that may be made of the information contained therein.

**Author Contributions:** Nicoletta Roberto conceived the manuscript and designed the algorithm, supported by Andrea Garzelli. Alberto Lupidi designed the numerical model scenario. Fabrizio Cuccoli and Elisa Adirosi participated in discussions of the results. Luca Baldini contributed useful suggestions and wrote the paper. Luca Facheris gave important guidance.

**Conflicts of Interest:** The authors declare no conflict of interest.

## Appendix A

In the framework of research activities developed in Clean Sky, a reference architecture has been defined that designates a decision support system (DSS) to host end-user applications using dual polarization measurements as input. Avionic devices acting as DSS on board of civil aircrafts must be certificated and must respect strict specifications (e.g., [39]). Often they have relatively poor performances in terms of both computational and storage capabilities with respect to computers for personal productivity. In order to test the SVM on a certified avionic DSS, we selected the EFB by Astronautics NEXIS Flight-Intelligence System co. [39], which has been taken as a reference. The EFB is composed by a display unit and a processing unit whose details are listed in Table A1. Classification output can be both displayed to the pilot, either associated to the label of hydrometeors (or to a set of new labels) or associated to a level of risk related to the presence of a given type of hydrometeor [40]. The risk map can be used by a Quasi-Artificial Intelligence (indicated as “Q-AI”) module that calculates the optimal route [41]. The procedure for hydrometeor classification processing for avionic weather radar measurements must satisfy some mandatory requirements in terms of processing time. Among all the avionic radar data processing tasks, the hydrometeor classification algorithm is the most demanding one in terms of processing time. Assume, for instance, that the aircraft speed is approximately  $800 \text{ km h}^{-1}$  and that the radar antenna sweeps  $120^\circ$  in azimuth with  $3^\circ$  angular resolution in 10 s, with 150 km of maximum range and 150 m range resolution. Each sweep implies 1000 range bins for about 40 azimuth lines implying labeling 1000 samples at least every 250 ms, or equivalently, at least  $4000 \text{ labels s}^{-1}$ . To evaluate the impact of these parameters on the performance and real-time operational condition, a benchmark test was performed by comparing a MATLAB implementation of FL classification and of the SVM HCA algorithm as adopted in this paper: the first generates only approximately 1200 labels/s and the latter 7000 labels/s (running on an x86\_64

Linuxmachine Eight core, Intel-i7@2,80GHz processor). These results highlight the SVM algorithm capability in terms of computational time and indicate it as a candidate for hydrometeors classification on anEFB machine.

**Table A1.** Astronautics' NEXIS EFB characteristics.

CPU	2 GHz Core i7 Intel
Display Touch Screen	8" XGA 1024 × 768 Pixels
Memory	4GB DDR3 1066 MHz
Ethernet	4 full duplex Ethernet channels (10/100 Base)
USB ports	1 USB port on display unit, 2 USB ports on electronic unit
Operating System	Certified Linux Operating System, DO178 Level C

## Appendix B

In this appendix, some considerations on the definitions of hydrometeor classes in WRF is given to fully understand the reference product used to validate the SVM HCA algorithm.

Given the different origin and definition of the WRF and HCA classes, different behaviors in terms of radar polarimetric measurements distribution at different heights are expected. In order to show that, we have carried out a "response test" in terms of radar polarimetric measurements. For this test, the WRF scenario described in Section 3.1 is considered and the hydrometeors are classified both by using WRF classification in the six classes (WRF-class) and by using the SVM HCA algorithm, starting from ideal polarimetric radar measurements. Figure A1 shows the histogram of  $Z_h$ , whose values are divided into the six classes classified by WRF-class at eight different heights for the whole event. The vertical distribution shows the presence of *rain* below the melting layer (ML,  $0^\circ$  isotherm is at 3900 m). Just below the ML, at 3000 m also *wet snow*, *dry snow*, *hail* and *hail mix* are found; at 3900 m into the ML *rain* and *hail* are not present while occurrences of *dry snow* increases and a peak of *graupel* occurrences appears; above the ML *drysnow* and *graupel* are found. Since the SVM HCA is trained using the physical assumptions made by the FL scheme, the response test on classes is evaluated from the output of FL classification. The histograms shown in Figure A2 for  $Z_h$  are obtained by classifying the WRF scenario using the FL classifier. The main notable differences of the FL output with respect to the WRF-class are: (i) the presence of *hail mix* below the ML and close to ground (at 150 m, 1500 m and 2250 m); (ii) the high number of occurrences of *wet snow* at ML height respect to *dry snow*; (iii) the presence of *graupel* just below (at 2250 m and 3000 m) and within the ML (at 3900 m); (iv) the *hail* class never appears. In terms of  $Z_h$  values for each class, the two classifications are fairly similar. Some differences are: *hail mix* has  $Z_h$  values between 40 and 60 dBZ below the ML for FL classifications that are covered only by *rain* in WRF classification; some *rain* occurrences have  $Z_h$  values less than 10 dBZ in WRF classification. These differences are mainly due to the definition of classes, in fact in WRF microphysics *hail*, *graupel*, and *snow*, are defined as dry hydrometeors (that means that are composed as a mixture of air and ice), while in FL classes *hail* and *graupel* classes includewet hydrometeors (defined as a mixture of air, ice and water). The dry hydrometeors are typically found only above the ML or just around it. In fact, the presence of *hail mix* and *graupel* below the ML for FL classifications is due to the presence of wet hydrometeors. The same tests were performed for  $Z_{dr}$  (not shown). The  $Z_{dr}$  values for each class are very similar in the two classification schemes. Main differences in vertical distributions of classes are the same shown in  $Z_h$  histograms. Nevertheless, the difference on polarimetric radar measurements response found in the two set of classes, mainly due to the composition of the hydrometeors, we can consider the WRF-class enough skilled to validate the SVM HCA algorithm. It is worth noting that the differences highlighted in this analysis are fundamental for the evaluation of validation results that are discussed in Section 3.3.

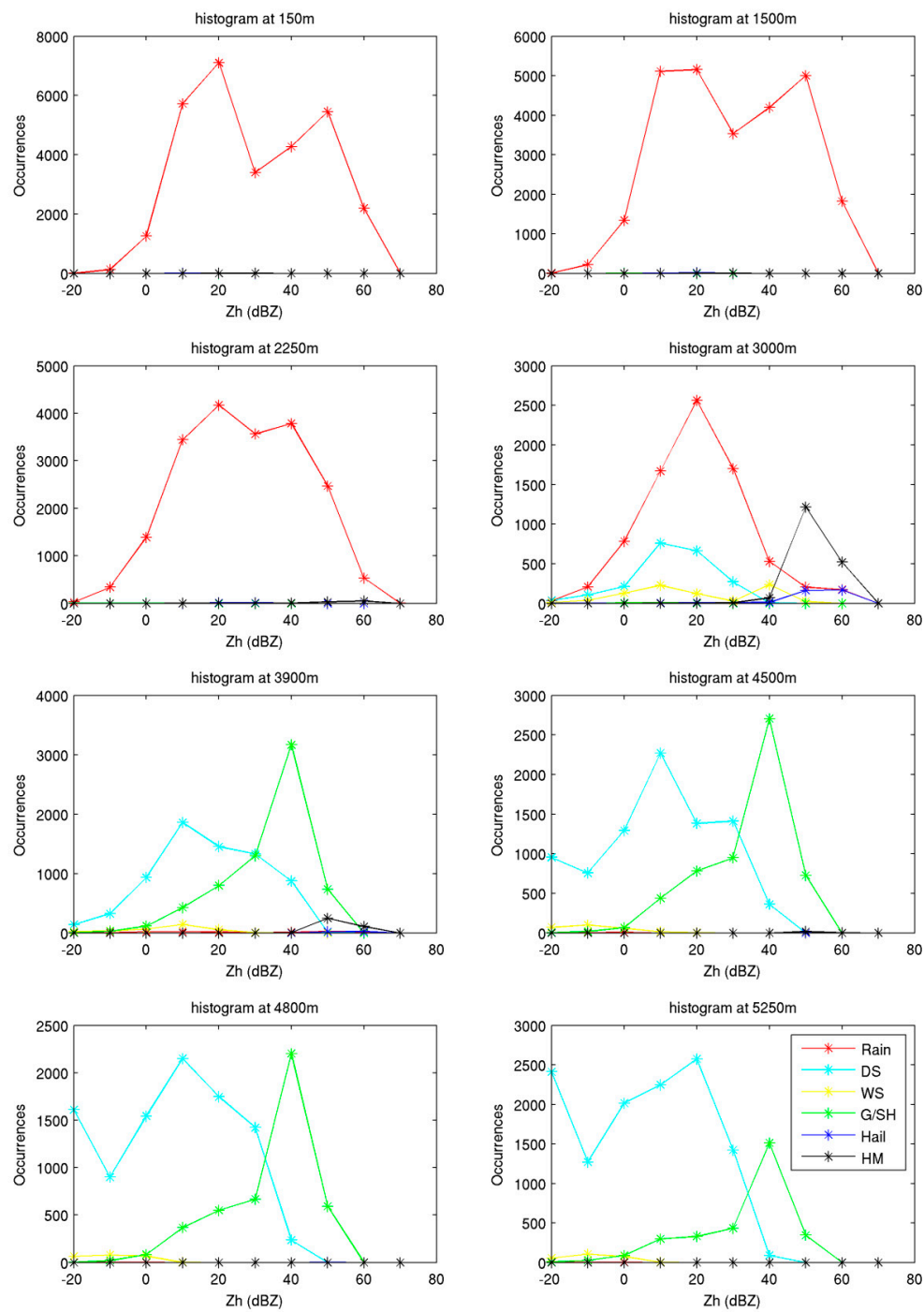


**Figure A1.** Histograms of  $Z_h$  for samples of the WRF scenario at different heights for the six hydrometeors classified using the WRF mixing ratio, as shown in Table 1. In the legend, DS, WS, G/SH, and HM mean *dry snow*, *wet snow*, *graupel/small hail*, and *hail mix*, respectively.

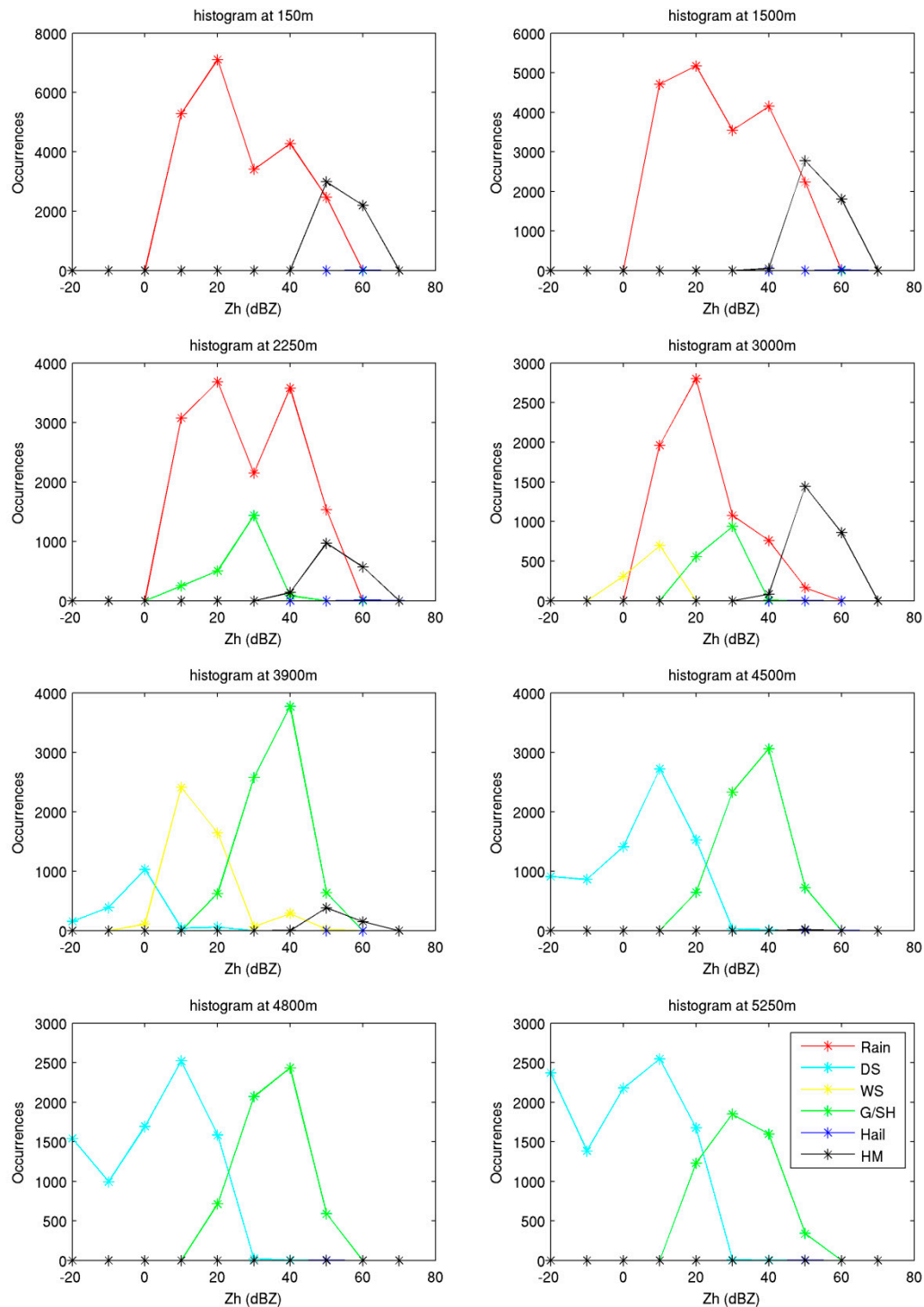


Figure A2. As for Figure A1, but the classification method is FL.

## References

1. Liu, H.; Chandrasekar, V. Classification of hydrometeor type based on multiparameter radar measurements: Development of a fuzzy logic and neuro fuzzy systems and in-situ verification. *J. Atmos. Ocean. Technol.* **2000**, *17*, 140–164. [\[CrossRef\]](#)
2. Straka, M.; Zrnica, D.S.; Ryzhkov, A.V. Bulk hydrometeor classification and quantification using polarimetric radar data: Synthesis of relations. *J. Appl. Meteorol.* **2000**, *39*, 1341–1372. [\[CrossRef\]](#)



3. Dolan, B.; Rutledge, S.A. A theory-based hydrometeor identification algorithm for X-band polarimetric radars. *J. Atmos. Ocean. Technol.* **2009**, *26*, 2071–2088. [[CrossRef](#)]
4. Dolan, B.; Rutledge, S.A.; Lim, S.; Chandrasekar, V.; Thurai, M. A robust C-band hydrometeor identification algorithm and application to a long-term polarimetric radar dataset. *J. Appl. Meteorol. Climatol.* **2013**, *52*, 2162–2186. [[CrossRef](#)]
5. Zrnić, D.S.; Ryzhkov, A.; Straka, J.; Liu, Y.; Vivekanandan, J. Testing A Procedure for Automatic Classification of Hydrometeor Types. *J. Atmos. Ocean. Technol.* **2001**, *18*, 892–913. [[CrossRef](#)]
6. Marzano, F.S.; Scaranari, D.; Vulpiani, G.; Montopoli, M. Supervised classification and estimation of hydrometeors using C-band dual-polarized radars: A Bayesian approach. *IEEE Trans. Geosci. Remote Sens.* **2008**, *46*, 85–98. [[CrossRef](#)]
7. Al-Sakka, H.; Boumahmoud, A.A.; Fradon, B.; Frasier, S.J.; Tabary, P. A new fuzzy logic Hydrometeor Classification Scheme applied to the French X-, C-, and S-band polarimetric radars. *J. Appl. Meteorol. Climatol.* **2013**, *52*, 2328–2344. [[CrossRef](#)]
8. Thompson, E.J.; Rutledge, S.A.; Dolan, B.; Chandrasekar, V.V.; Cheong, B. A Dual-Polarization Radar Hydrometeor Classification Algorithm for Winter Precipitation. *J. Atmos. Ocean. Technol.* **2014**, *31*, 1457–1481. [[CrossRef](#)]
9. Roberto, N.; Adirosi, E.; Baldini, L.; Casella, D.; Dietrich, S.; Gatlin, P.; Panegrossi, G.; Petracca, M.; Sanò, P.; Tokay, A. Multi-sensor analysis of convective activity in central Italy during the HyMeX SOP 1.1. *Atmos. Meas. Technol.* **2016**, *9*, 535–552. [[CrossRef](#)]
10. Bechini, R.; Chandrasekar, V. A semisupervised robust hydrometeor classification method for dual-polarization radar applications. *J. Atmos. Ocean. Technol.* **2015**, *32*, 22–47. [[CrossRef](#)]
11. Grazioli, J.; Tuia, D.; Berne, A. Hydrometeor classification from polarimetric radar measurements: A clustering approach. *Atmos. Meas. Tech.* **2015**, *8*, 149–170. [[CrossRef](#)]
12. Besic, N.; Figuerasi Ventura, J.; Grazioli, J.; Gabella, M.; Germann, U.; Berne, A. Hydrometeor classification through statistical clustering of polarimetric radar measurements: A semi-supervised approach. *Atmos. Meas. Tech.* **2016**, *9*, 4425–4445. [[CrossRef](#)]
13. Mountrakis, G.; Im, J.; Ogole, C. Support vector machines in remote sensing: A review. *ISPRS J. Photogramm. Remote Sens.* **2011**, *66*, 247–259. [[CrossRef](#)]
14. Lee, Y.; Wahba, G.; Ackerman, S.A. Cloud classification of satellite radiance data by multicategory support vector machines. *J. Atmos. Ocean. Technol.* **2004**, *21*, 159–169. [[CrossRef](#)]
15. Grazioli, J.; Tuia, D.; Monhart, S.; Schneebeli, M.; Raupach, T.; Berne, A. Hydrometeor classification from two-dimensional video disdrometer data. *Atmos. Meas. Tech.* **2014**, *7*, 2869–2882. [[CrossRef](#)]
16. Yanovsky, F.; Ostrovsky, Y.; Marchuk, V. Hydrometeor Type and Turbulence Intensity Recognition with Doppler-Polarimetric Radar. In Proceedings of the Radar Conference, Amsterdam, The Netherlands, 30–31 October 2008.
17. Lim, S.; Chandrasekar, V.; Bringi, V.N. Hydrometeor classification system using dual-polarization radar measurements: Model improvements and in situ verification. *IEEE Trans. Geosci. Remote Sens.* **2005**, *43*, 792–801. [[CrossRef](#)]
18. Roberto, N.; Baldini, L.; Adirosi, E.; Lischi, S.; Lupidi, A.; Cuccoli, F.; Barcaroli, E.; Facheris, L. Test and validation of particle classification based on meteorological model and weather simulator. In Proceedings of the 13th European Radar Conference (EuRAD), London, UK, 11–13 October 2016.
19. Lupidi, A.; Lischi, S.; Berizzi, F.; Cuccoli, F.; Roberto, N.; Baldini, L. Validation of the advanced polarimetric Doppler weather radar simulator with Polar55C Real Observations. In Proceedings of the 15th International Radar Symposium (IRS), Gdansk, Poland, 16–18 June 2014.
20. Lischi, S.; Lupidi, A.; Martorella, M.; Cuccoli, F.; Facheris, L.; Baldini, L. Advanced Polarimetric Doppler Weather Radar Simulator. In Proceedings of the 15th International Radar Symposium (IRS), Gdansk, Poland, 16–18 June 2014.
21. Scholkopf, B.; Smola, A.J. *Learning with Kernels: Support Vector Machines, Regularization, Optimization, and Beyond*; MIT Press: Cambridge, MA, USA, 2001.
22. Boser, B.E.; Guyon, I.; Vapnik, V. A training algorithm for optimal margin classifiers. In Proceedings of the Fifth Annual Workshop on Computational Learning Theory, Pittsburgh, PA, USA, 27–29 July 1992.
23. Cortes, C.; Vapnik, V. Support-vector network. *Mach. Learn.* **1995**, *20*, 273–297. [[CrossRef](#)]

24. Hastie, T.; Tibshirani, R.; Friedman, J. *The Elements of Statistical Learning*, 2nd ed.; Springer: New York, NY, USA, 2008.
25. Chang, C.C.; Lin, C.J. LIBSVM: A Library for Support Vector Machines. Available online: <http://www.csie.ntu.edu.tw/~cjlin/libsvm> (assessed on 21 June 2017).
26. Baldini, L.; Gorgucci, E.; Chandrasekar, V.; Peterson, W. Implementations of CSU Hydrometeor Classification Scheme for C-Band Polarimetric Radars. Available online: [https://ams.confex.com/ams/32Rad11Meso/techprogram/paper\\_95865.htm](https://ams.confex.com/ams/32Rad11Meso/techprogram/paper_95865.htm) (assessed on 21 June 2017).
27. Vulpiani, G.; Baldini, L.; Roberto, N. Characterization of Mediterranean hail-bearing storms using an operational polarimetric X-band radar. *Atmos. Meas. Tech.* **2015**, *8*, 4681–4698. [CrossRef]
28. Bringi, V.N.; Chandrasekar, V. *Polarimetric Doppler Weather Radar: Principles and Applications*; Cambridge University Press: Cambridge, UK, 2005.
29. Vulpiani, G.; Montopoli, M.; DelliPasseri, L.; Gioia, A.; Giordano, P.; Marzano, F.S. On the use of dual-polarized C-band radar for operational rainfall retrieval in mountainous areas. *J. Appl. Meteorol. Climatol.* **2012**, *51*, 405–425. [CrossRef]
30. Adirosi, E.; Baldini, L.; Roberto, N.; Vulpiani, G.; Russo, F. Using disdrometer measured raindrop size distributions to establish weather radar algorithms. In *AIP Conference Proceedings*; AIP Publishing: Melville, NY, USA, 2015; pp. 110–128.
31. Baldini, L.; Roberto, N.; Gorgucci, E.; Fritz, J.; Chandrasekar, V. Analysis of dual polarization images of precipitating clouds collected by the COSMO SkyMed constellation. *Atmos. Res.* **2013**, *144*, 21–37. [CrossRef]
32. Michalakos, J.; Dudhia, J.; Gill, D.; Henderson, T.; Klemp, J.; Skamarock, W.; Wang, W. The Weather Research and Forecast Model: Software Architecture and Performance. In *Use of High Performance Computing in Meteorology, Proceedings of the 11th ECMWF Workshop on the Use of High Performance Computing in Meteorology; Reading, England, October 2004*; World Scientific: Singapore, 2005.
33. Milbrandt, J.A.; Yau, M.K. A multimoment bulk microphysics parameterization. Part I: Analysis of the role of the spectral shape parameter. *J. Atmos. Sci.* **2005a**, *62*, 3051–3064. [CrossRef]
34. Milbrandt, J.A.; Yau, M.K. A multimoment bulk microphysics parameterization. Part II: A proposed three-moment closure and scheme description. *J. Atmos. Sci.* **2005b**, *62*, 3065–3081. [CrossRef]
35. Montopoli, M.; Roberto, N.; Adirosi, E.; Gorgucci, E.; Baldini, L. Investigation of Weather Radar Quantitative Precipitation Estimation Methodologies in Complex Orography. *Atmosphere* **2017**, *8*, 34. [CrossRef]
36. Sebastianelli, S.; Russo, F.; Napolitano, F.; Baldini, L. On precipitation measurements collected by a weather radar and a rain gauge network. *Nat. Hazards Earth Syst. Sci.* **2013**, *13*, 605–623. [CrossRef]
37. Haralick, R.M.; Shanmugam, K.; Dinstein, I. Textural Features for Image Classification. *IEEE Trans. Syst. Man Cybern.* **1973**, *6*, 610–621. [CrossRef]
38. Haralick, R.M.; Linda, G.S. *Computer and Robot Vision*; Addison-Wesley Longman: Boston, MA, USA, 1992; pp. 28–48.
39. Federal Aviation Administration: Guidelines for the Certification, Airworthiness, and Operational Use of Electronic Flight Bags. Available online: [https://www.faa.gov/documentLibrary/media/Advisory\\_Circular/AC\\_120-76C.pdf](https://www.faa.gov/documentLibrary/media/Advisory_Circular/AC_120-76C.pdf) (assessed on 21 June 2017).
40. Sermi, F.; Cuccoli, F.; Mugnai, C.; Facheris, L. Aircraft hazard evaluation for critical weather avoidance. *MetroAeroSpace* **2015**. [CrossRef]
41. Serafino, G. Multi-objective Aircraft Trajectory Optimization for Weather Avoidance and Emissions Reduction. In *International Workshop on Modelling and Simulation for Autonomous Systems*; Springer: Cham, Switzerland, 2015; pp. 226–239.

